Wastewater Treatment In Large-scale Novel Corrugated-Sheet MBR

Yuan Fang[a1], Dengyue Chen[b1], Yan Zhang[a], Robert Field[d,e] Jun Jie Wu[e*], Bing Wang[a*],

[a] *College of Environmental Science and Engineering/Sino-Canada Joint R&D Centre for Water and Environmental Safety, Nankai University, Tianjin 300071, PR China*

[b] *School of Pharmaceutical Sciences, Xiamen University, Xiamen 361005, Fujian, PR China*

[c] *Faculty of Engineering and Environment, Northumbria University, Newcastle NE1 8ST, UK*

[d] *Department of Engineering Science, University of Oxford, Oxford OX1 3PJ, UK*

[e] *Department of Engineering, Faculty of Science, Durham University, Durham DH1 3LE, UK*

[#] Y Fang and D Chen contributed equally to this work and should be considered as co-first authors.

* Corresponding authors: J J Wu, junjie.wu@durham.ac.uk and B Wang, bwang@nankai.edu.cn

Abstract

This is a threefold study concerning a novel corrugated-sheet MBR. Besides the optimization of the hydrodynamics and of air consumption to achieve excellent amelioration of fouling, this study introduces a novel corrugated sheet (CS) membrane to the research community. The CS membrane has a general plate configuration similar to a standard flat sheet (FS) membrane but at 1.6 mm thickness, it is much thinner. The rows of hemispherical hollow units on each side create corrugations, and coupled with the thinness of the plate they give a surface area per unit volume value around that of hollow fiber systems. The hydrodynamics and fouling of the CS membrane were compared with those of FS membrane through computational fluid dynamics (CFD) simulation and experiments. Based upon these results a large-scale corrugated sheet membrane bioreactor (CS-MBR) with four decks was designed. The study included a consideration of three different designs of aerators, the spacing between the decks and the aeration rate. With the recommended partitioning design of aerator, the optimized nozzle velocity was found to be 13 m/s corresponding to a world-leading specific aeration demand, SAD_m (aeration amount per unit membrane area per unit time), of 0.074 $Nm^3m^{-2}h^{-1}$. This corresponds to a 70% reduction with respect to a FSMBR operated with slug bubbling and is just one-eighth of the traditional industrial usage of 0.3 to 0.58 $Nm^3m^{-2}h^{-1}$ depending on format of the system.

Key Words

Corrugated sheet (CS) membrane; Large-scale MBR; CFD; Fouling control; Air consumption.

1. Introduction

Membrane bioreactors (MBR) are an efficient device which have replaced the secondary sedimentation process in wastewater treatment [1]. However, fouling remains a critical issue that reduces membrane performance [2-4]. At present, the main method to attenuate membrane fouling is the use of aeration to scour membrane surface [5-7], but consequently there is a corresponding high energy consumption [8-10] which impedes the wider adoption of MBRs [11, 12].

Both flat sheet (FS) and hollow fiber (HF) MBRs have been commonly used in industry over the past two decades [8, 13-16]. It is well known that for FS-MBR system is easy to maintain with only a small amount of sludge sedimentation but on the other hand, the loading capacity is low and normally backwash cannot be conducted. Although the HF membrane module overcomes these two shortcomings, there is the issue of “hair twinning” i.e. the binding together of filaments caused by constituents in the sewage, and this causes dead zones, poor hydraulic circulation and hence heavily fouling [17].

Thus, in order to improve the normal membrane features, some researches have recently focused on variations to the membrane format in order to reduce membrane fouling and improve filtration performance. One approach has been to physically press PVDF flat sheet membranes to generate a corrugated surface structure [18]. This was explored in the context of seawater desalination process, and flux was higher and there was less salt deposition on the membrane surface. Whilst the corrugation of the membrane surface is expected to ameliorate fouling, simply corrugating the membranes in a traditional system (if this were possible) would still lead to the retention of a major constraint, namely the relatively small surface area per unit volume that is inherent in FSMBR systems compared with hollow fiber ones. To address this issue, a novel type of corrugated sheet (CS) membrane was recently proposed and is now produced and assembled as an MBR system for industrial application (Beijing Origin Water Membrane Technology Co. Ltd, Beijing, China). As shown in Figure 1, this new type of CS membrane consists of a very thin polyethylene terephthalate (PET) flat central sheet that is just 90 μm thick and hemispherical channels on either side. The overall thickness is 1.6 mm which is similar to that of hollow fibers. With these dimensions the loading capacity is improved and the CS-MBR system can achieve surface area per unit volume values close to 400 m^2/m^3 which is superior to both the value of 256 m^2/m^3 [19] and the value of 300 m^2/m^3 used by Cranfield as a standard for hollow fiber MBR systems [20].

The strength of the CS sheets enables them to be mounted so that the bubble flow is transverse to the corrugated surface. Thus the flow creates beneficial ripples. It is well known that the combination of (i) unsteady flow or oscillatory flow with (ii) baffles or corrugations increases mass transfer at surfaces and inhibits fouling [21, 22, 23] and this is discussed further in section 3.4. Moreover, the arrangement of the CS sheets enables the permeate to be conveyed horizontally through the hemispherical hollow fibers so that the permeate collection can be on both sides. This arrangement enables more and better MBR configurations such as multiple decks; 4 ~ 6 decks are normal with a corrugated sheet membrane bioreactor (CS-MBR). The multi decks are served by the same aeration pipe which significantly reduces the air consumption; for MBRs this is the important operating cost and the level of consumption (measured in units of $Nm^3m^{-2}h^{-1}$ i.e. volume per unit area per unit time) has often been the most important issue faced in large-scale MBR application in industry [24].

Currently, this new CS-MBR is applied into large-scale water treatment in Beijing, Taiyuan and Shaanxi province of China. The corrugation on membrane surface in the new CS-MBR creates hydrodynamic flows that are at least as complex as the flow in normal FSMBR [25-28]. Moreover, it has been unclear how hydrodynamics and fouling control effect varied in CS-MBR comparing to those obtained in FSMBR [19, 29]. Thus a fundamental study was undertaken to examine the fluid dynamics and fouling in CS-MBR systems.

As CS-MBR systems are relatively new, they have yet to be studied in detail. Issues addressed in our study included the aeration system and the spacing between decks. The spacing is known to influence the two-phase flow in the upper part [30]. Moreover, although there is a link between the hydrodynamics and fouling [31-34], it is important to assess if the new design created unexpected dead-zones which might cause unexpected fouling. Thus our study included an experimental examination of fouling. Other components were CFD simulations and electro-diffusion (EDM) studies [35]. Finally, the aeration usage was calculated and compared, which could provide a reference for the practical application of CS-MBR in industry.

2. Methods

The corrugated membrane is made of PVDF material with an internal supporting PET plate as shown in Fig. 1. Due to the special structure, between the membrane and PET plate, the corrugated hemispheres form independent permeate channels. These channels are connected to the water collection system that is operated under suction. As water is collected on both sides there is a reduced path length. This, together with the excellent water permeability, permits operation at a reduced TMP; the level is around two-thirds of the value needed in traditional MBRs.

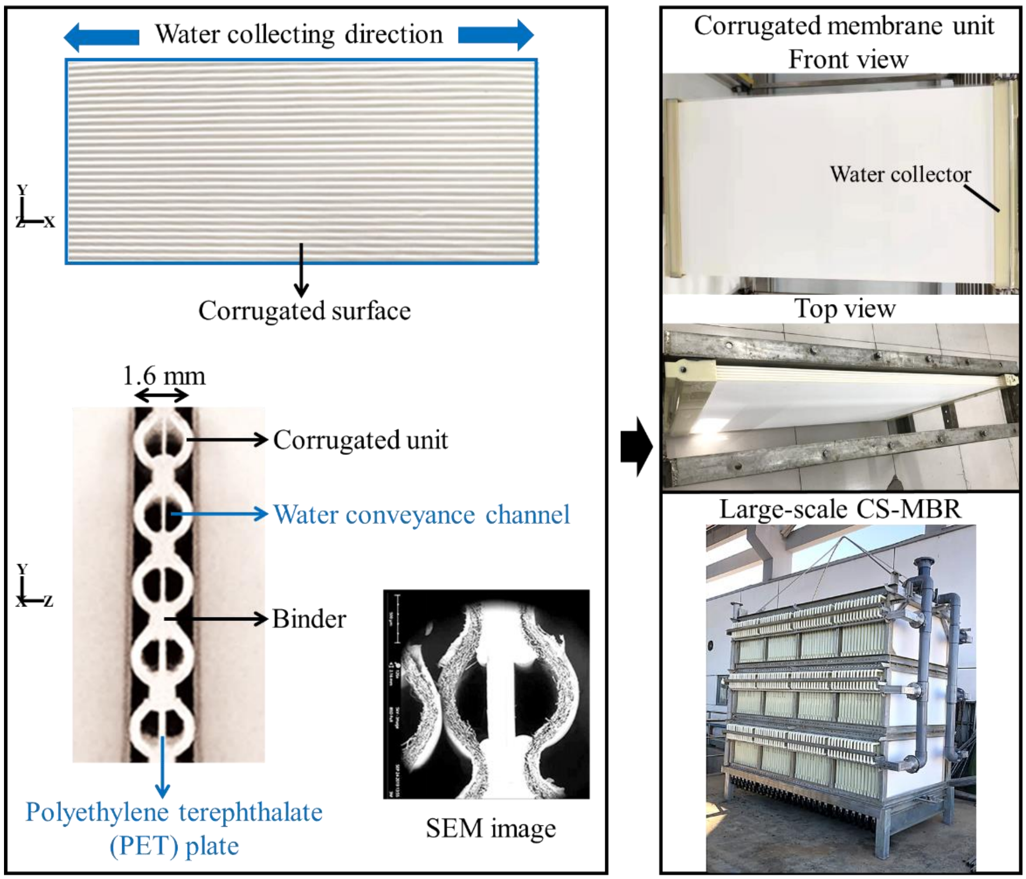

Fig. 1 Schematic diagram and the prototype of corrugated membrane and large-scale CS-MBR system at various orientations.

2.1 Experimental method

2.1.1 Shear stress measurement

Shear stress was measured for nine positions using the electro-diffusion method (EDM) [7, 36] in two plexiglass tanks of FS and CS respectively, as shown in Fig. 2 with dimensions of 180 × 70 × 5 mm. An air nozzle of diameter 3 mm at the base of the tank bottom provided aeration of 1 L/min. The fouling experiment was carried out in a larger rectangular bio-reactor tank measuring 750 × 350 ×120 mm. Two membrane modules of FS and CS (Origin Water Co. Ltd, China) were immersed in the reactor with effective filtration area of 0.1 m^2. The aeration conditions were same for both modules with 2.5 L/min of aeration delivered with pulsing at 1 Hz. The pulsing of the air flow has previously been found to be beneficial [27, 28].

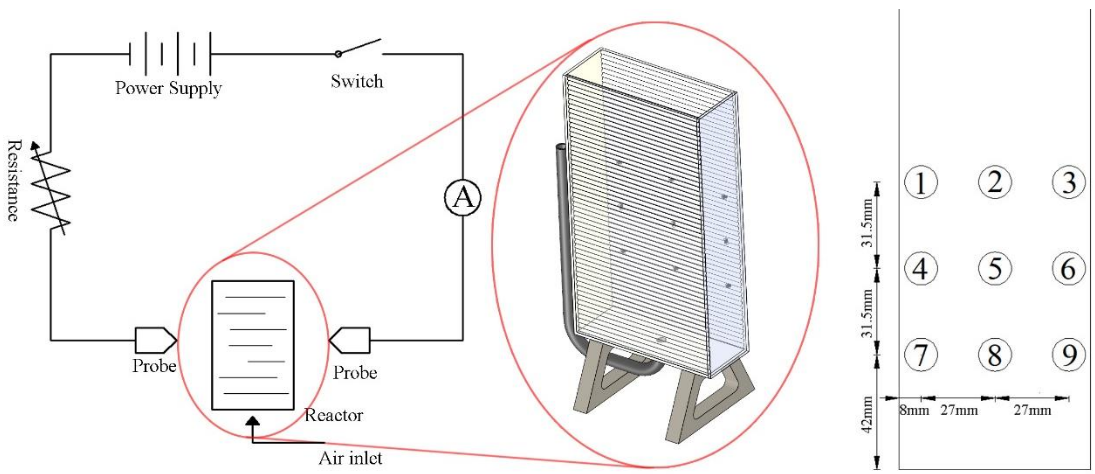

(a) (b)

Fig. 2 Schematic diagram of the EDM experimental rig: (a) electric circuit diagram; (b) nine positions for measurement on tank wall

The solution was prepared with ultrapure water, potassium ferrocyanide 0.01 M and sodium hydroxide 0.5 M. The experimental schematic diagram is shown in Figure 2 (a). 200 mV electricity was continuously supplied by a stabilized voltage supply, current was recorded by ammeter, and the rheostat resistance was set to be 100 ohms. Electrodes of platinum and nickel were used for the anode and cathode respectively. The latter were at nine positions on the walls in both tanks as shown in Fig. 2 (b). In section S1.1 of Supplementary Material, experimental method details are presented.

2.1.2 Fouling experiments

The experiment was carried out in a 750 × 350 ×120 mm rectangular bio-reactor tank. The operating liquid level was 700 mm controlled by a peristaltic pump. As shown in Fig. 3, two membrane modules were immersed in the reactor, one with FS membrane and the other with the CS one (Origin Water Co. Ltd, China). Effective filtration areas were 0.1 m^2. The aeration conditions were same for both modules. Aeration pipe was located 120 mm directly below the modules, with 2.5 L/min flow rate and 1 Hz frequency. During operation, permeate flux and transmembrane pressure (TMP) were recorded, the latter by digital pressure gauge. The experiments were conducted at room temperature. Activated sludge details could be found in Supplementary Material S1.2.

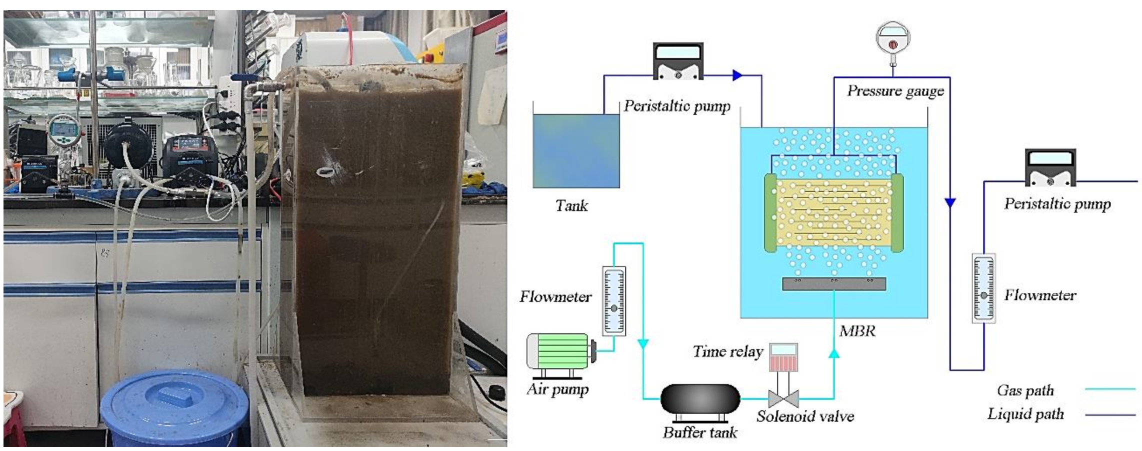

Fig. 3 Fouling experimental schematic of MBR module set-up

2.1.3 Aeration experiments

Additionally, new configurations of aeration pipe were initially designed and compared with the traditional one. Slug bubbling process could be achieved via solenoid valve. Air flow rate was fixed at 78 L/min and bubble frequency at 1 Hz. Detail information is shown in Supplementary Materials Section S1.3.

2.2 CFD simulation method

The aeration device was designed as a cuboid box whose bottom had been removed, as shown in Figure S2. During aeration, the air entered the aeration box and its pressure displaced some of the liquid causing a liquid level to form within the box. The air flowed out from the nozzles. (The drop in liquid level is related to the pressure drop across the aeration holes). In this design, there were 14 nozzles on each side of the aeration box, spaced as pairs with a gap of 12 mm. Other dimensions are shown in Figure S2 (a).

2.2.1 Governing equations

Gas-liquid two-phase flow was simulated in ANSYS FLUENT 14.5. Pressure-based solver with PISO scheme for pressure-velocity coupling was set for calculation. Aeration rate at each nozzle was varied between 10 ~ 16 m/s. Major equations for mass and momentum conservation were given below:

$$\frac{\partial \rho}{\partial t} + \nabla(\rho \vec{u}) = 0 \tag{1}$$

$$\frac{\partial}{\partial t}(\rho \vec{u}) + \nabla(\rho \vec{u}\vec{u}) = -\nabla P + \rho \vec{g} + \rho \vec{F} + \nabla \vec{\tau} \tag{2}$$

where

$$\rho = \sum \alpha_q \rho_q \tag{3}$$

$$\mu = \sum \alpha_q \mu_q \tag{4}$$

$$\sum_{q=1}^{n} \alpha_q = 1 \tag{5}$$

Amongst turbulence models, the Realizable *k*–*ε* model was chosen because of its utility for complex bubble behavior calculation. It can be expressed as:

$$\frac{\partial}{\partial t}(\rho k) + \frac{\partial}{\partial x_j}\left(\rho k u_j\right) = \frac{\partial}{\partial x_j}\left[\left(\mu + \frac{\mu_t}{\sigma_k}\right)\frac{\partial k}{\partial x_j}\right] + G_k + G_b - \rho\varepsilon - Y_M \tag{6}$$

$$\frac{\partial}{\partial t}(\rho \varepsilon) + \frac{\partial}{\partial x_j}\left(\rho \varepsilon u_j\right) = \frac{\partial}{\partial x_j}\left[\left(\mu + \frac{\mu_t}{\sigma_\varepsilon}\right)\frac{\partial \varepsilon}{\partial x_j}\right] + \rho C_1 S\varepsilon - \rho C_2 \frac{\varepsilon^2}{k + \sqrt{\upsilon\varepsilon}} + C_{1\varepsilon}\frac{\varepsilon}{k} C_{3\varepsilon} G_b + S_\varepsilon \tag{7}$$

where

$$\mu_t = \rho C_\mu \frac{k^2}{\varepsilon}$$

$$C_1 = \max\,[0.43, \frac{\eta}{\eta + 5}]$$

$$\eta = S\frac{k}{\varepsilon}$$

$$S = \sqrt{2 S_{ij} S_{ij}}$$

$$G_k = -\rho\,\overline{u_i' u_j'}\,\frac{\partial u_j}{\partial x_i}$$

$$G_b = \beta g_i \frac{\mu_t}{Pr_t}\frac{\partial T}{\partial x_i}$$

The Continuum Surface Force (CSF) model was used for surface tension calculation. This is structured as:

$$p_L - p_G = \sigma\kappa \tag{8}$$

$$\vec{F}_{vol} = \sigma \frac{2\rho\kappa\nabla_{\alpha_G}}{(\rho_L + \rho_G)} \tag{9}$$

$$\kappa = \nabla\hat{n}$$

$$\hat{n} = \frac{n}{|n|}, n = \nabla\alpha_q$$

2.2.2 Numerical methods and boundary conditions

The simulations were carried out using a pressure-based solver in commercial code ANSYS FLUENT 14.5. Liquid water was chosen as liquid phase, which density is 998.2 kg/m^3 and viscosity is 0.001003 Pa·s. Air was chosen as gas phase, density 1.225 kg/m^3 and viscosity 0.000017894 Pa·s. The mass transfer process and membrane water permeability were not considered in the simulation. A second order upwind scheme was chosen for momentum and k–ε equations discretization. PRESTO! (pressure staggering option) scheme was adopted for pressure term calculation. The aeration pipe outside wall is one of the wall boundary conditions and the gas inlet is set to be inlet, whilst the outflow condition was set at the air nozzle boundary. The boundaries for walls were all stationary and there was a no fluid-slip condition at the membrane surface

The important assumption is the membrane sheets were considered to be “rigid walls”. In other words, the membrane is assumed to be inflexible sheets, which could not bend which is a little different from the actual situation. Additionally the influence of membrane permeation upon shear stress calculation is neglected; a decision that is supported by order of magnitude calculation..

Details for CFD simulation method was given in Section S2.2 of Supplementary Materials, consisting of numerical geometry, mesh detail, simulation models and equations. Figure S4 gives the typical mesh example.

3. Results and discussion

Before considering large-scale design of CS-MBR systems in section 3.2, and air consumption of the CS-MBR with that of other MBRs in section 3.3, a two-fold experimental comparison of CS and FS membranes is made. After examining the shear stress generated on the membrane surfaces, the experimental findings regarding the propensity of those surfaces to fouling are presented.

3.1 Experimental comparison of CS and FS membrane

3.1.1 Shear stress comparison

The fouling mitigation is closely related to shear stress, which has been studied in multiple previous work [7, 19, 28]. Hence the shear stress induced by two-phase flow was carefully studied for the CS membrane format. Generally there are two methods for CFD model validation, one is to take photos by high-speed camera for the bubbles, as shown in our previous papers [39-41] and Leslie et al. [19]; the other is to measure shear stress and compare [17]. Both validation methods ware recommended and sufficient for the two-phase flow CFD model. Although the gas-liquid flow model has been validated by bubble photos in our previous studies [39-41], shear stress was measured in this study in order to have robust measures for the two types of membranes.

In particular the shear stress distribution on the FS and CS membranes were obtained from CFD simulation and compared with EDM data as shown in Fig. 4. It is found that the error between simulation and EDM results is less than 8% for both CS and FS membrane, which indicated the CFD model is robust for hydrodynamics simulation. A preliminary study of grid independence was performed, an increase in the number of nodes was found to have essentially no effect. Also, it was found that the results of simulations based on the mesh shown in this work was in accordance with experimental results. Moreover, the comparison of simulation with experiment in Fig. 4 validates our simulation model.

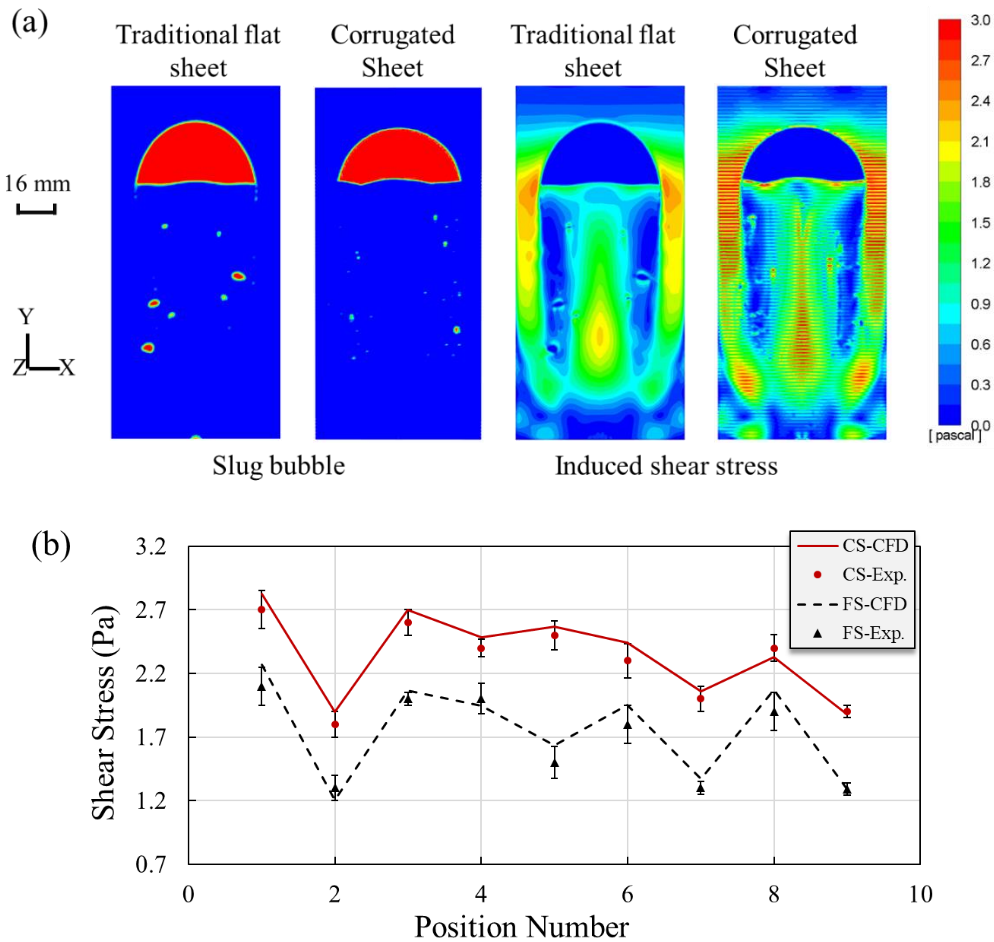

Fig. 4 Bubble morphology and shear stress distribution in FS and CS membrane: (a) results from CFD simulation; (b) shear stress comparison from both CFD and EDM experimental results.

Fig. 4 (a) shows that the bubble size is similar in both modules. However, there are differences for shear stress between the two surfaces, especially in the bubble rim and nose areas. The detail information of shear stress comparison is analyzed in Fig. 4 (b). It shows that the maximum shear stress at nine positions on FS is in the range of 1.3 ~ 2.3 Pa, which is similar with CFD prediction. As clearly shown, the shear stress on CS surface is higher than that on the FS surface; the former has values in the range of 1.8 ~ 3.0 Pa. The highest difference of shear stress between two modules is around 1 Pa at Position 5, corresponding to the bubble nose part. This is partially because the special ripple structure on the CS surface enhances the turbulence and hence the shear stress, as also detected in previously mentioned research [37]. One can conclude that the CS membrane is scoured more strongly than the FS one. The effect of the more intense hydrodynamics is further studied in the next section addressing fouling performance.

3.1.2 Fouling performance

The fouling experiments for both flat and corrugated membrane components were carried out for 360 hours, and Fig. 5 shows the performance data in terms of transmembrane pressure (TMP) and permeability. In Fig. 5 (a), the initial TMPs are relatively close, both of which are around 2 kPa. During the initial period from 0 to 50 h, the flat membrane has a relatively rapid increase in TMP, whilst that of CS increased at around half the rate. In the following 150 h, the rate of TMP increase is similar for both membranes; the offset of around 7.5 kPa is that which had be set during the first 50 h of operation. After 200 h, the rate of increase in TMP for both membranes are reduced. During this stage, fluctuations in the TMP are noticeable particularly for FS and the difference in TMP widened slightly to around 10 kPa. In general, it indicates that CS membrane fouled less than the FS membrane particularly during the initial period of operation.

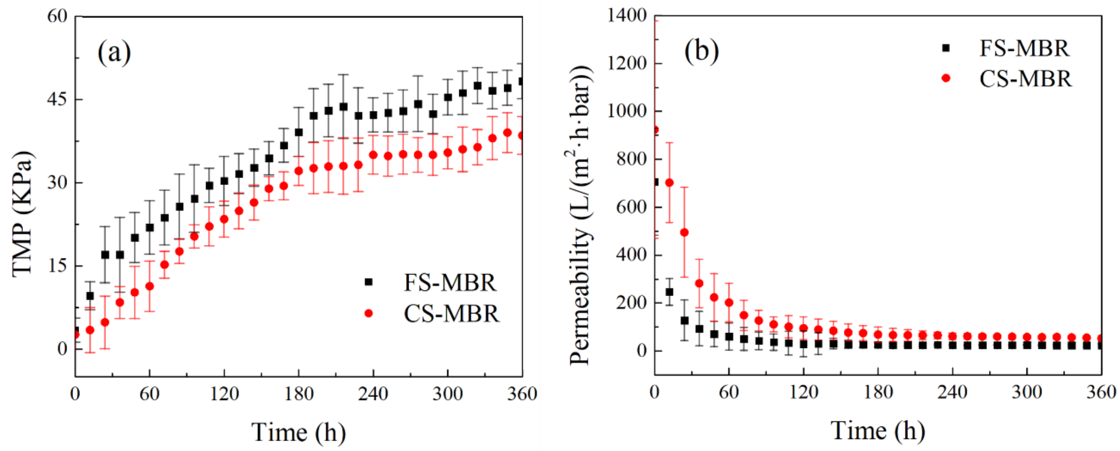

Fig. 5 Comparison of fouling performance between CS- and FS-MBR modules: (a) TMP variation; (b) Permeability results.

The evolution in permeability is displayed in Fig. 5 (b). The initial permeabilities are 700 and 920 L/(m^2·h·bar) for FS and CS respectively. During the first 150 h, both specific fluxes experienced rapid decline and in the final phase the permeabilities tended towards 100 and 50 L/(m^2·h·bar) for CS and FS respectively. Also it can be noted that beyond 250 h the rate of increase of TMP is distinctly lower for CS compared with FS. Clearly CS type in comparison with the FS one has features which generate improved hydrodynamics that ameliorate fouling, as discussed in section 3.1.1 of shear stress is key to fouling control [38].

3.2 Large-scale CS-MBR design

Given the above very promising results, a large-scale corrugated sheet membrane bioreactor (CS-MBR) with four decks was designed. Four decks are standard for most large-scale application of the CS-MBR but issues needing addressing were: (i) the aeration section needs to be optimized to achieve control of fouling whilst avoiding excessive aeration, (ii) the influence of the gap distance between different decks, and (iii) the influence of aeration rates / nozzle velocities. These three areas form the subsections of this section and then section 3.3 compares the air consumption of the optimized CS-MBR with that of other MBRs.

3.2.1 Aeration pipe design

Hydrodynamic behavior from three aeration pipe configurations was analyzed and compared through CFD and experiment. Assuming same velocity for each pair of nozzles, the 14 nozzles can be represented by seven groups. Hence the nozzle group number was ranked 1 ~ 7 from left to right of aeration pipe as shown in the abscissa of Fig. S2 (b). Inlet air flow rates were the same in all cases, and two rates were applied here, one was the traditional normal value used in industry of 10 L/min·m^2, the other was around half of this value at approximately 5 L/min·m^2. The air velocity of each nozzle from CFD simulation was plotted as function of nozzle number as shown in Fig. 6.

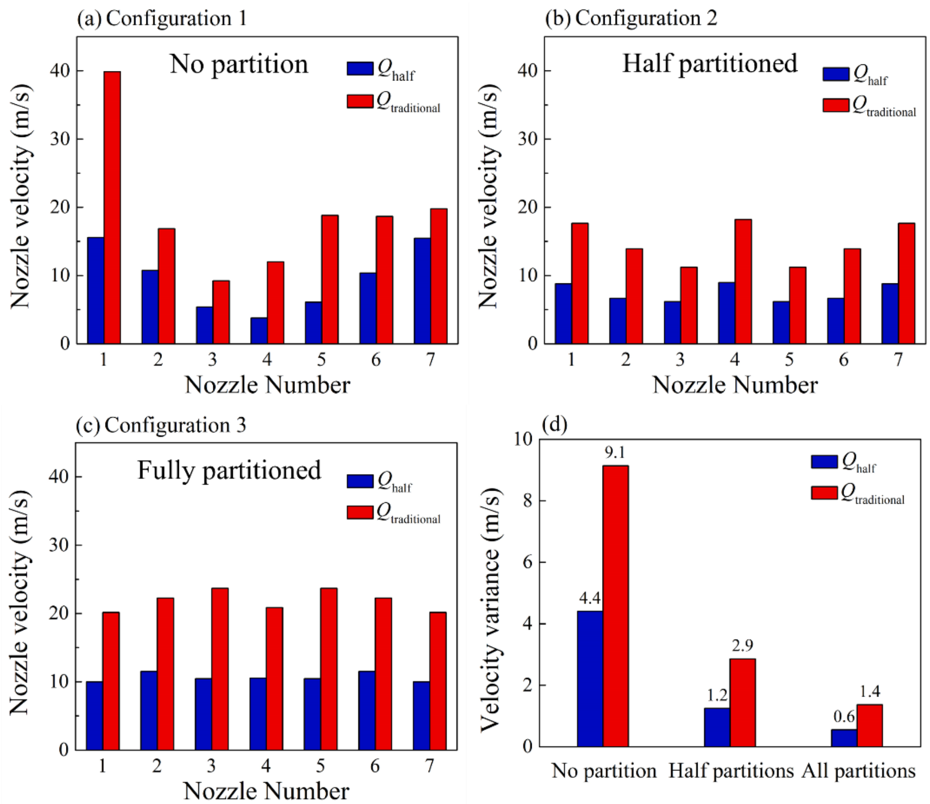

Fig. 6 Influence of aerator configurations upon the distribution of air nozzle velocities at two different overall inputs corresponding to 10 L/min·m^2 and other is *circa* 5 L/min·m^2: (a) no partition; (b) half partitioned; (c) fully partitioned; (d) velocity variance.

In Fig. 6 (a) to (c), the nozzle velocity distributions from three aeration pipe configurations are presented whilst in Fig. 6 (d), the velocity standard variance was calculated. For Configuration 1, at both flow rates, the velocity from nozzle 1 is much higher than from the others; furthermore that from nozzles 3 and 4 are much smaller than any of the other five nozzles. As shown in Fig. 6 (d), this configuration has the highest variance. Now when the aeration pipe is half partitioned or more fully partitioned, the velocity variation between different nozzles is reduced. The greater uniformity of flow is confirmed by the reduced variances in Fig. 6 (d), indicating as partitioning is increased the variance reduced. Thus, in Configuration 3 with fully partitioned, nozzle velocity has less fluctuation and the most uniform. As Configuration 2 structure is a simple one, both it and Configuration 3 were tested in further bubbling experiments.

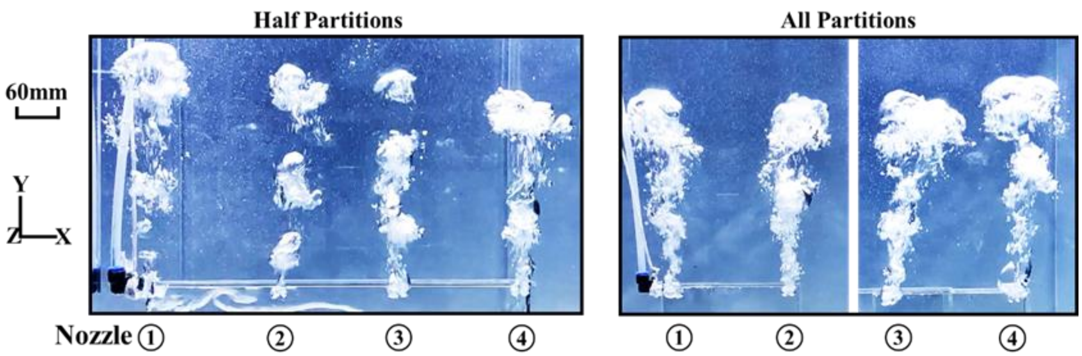

Fig. 7 Bubble size measurement in experiment for various aeration configurations.

Table 1 Bubble size (mm) measured in experiment for various aeration configurations.

	Configuration of Half Partitions		Configuration of All Partitions	
Nozzle Number	w_x	w_y	w_x	w_y
Nozzle 1	100±1	86±2	91±2	93±1
Nozzle 2	76±1	59±1	90±1	87±2
Nozzle 3	51±2	41±1	113±1	87±1
Nozzle 4	109±1	62±2	110±2	85±1
Standard variance	23	16	10	3

* w_x: bubble size measured in X-direction; w_y: bubble size measured in Y-direction.

Bubble behavior of two aeration devices (Configuration 2 and 3) was tested, and the bubble size was measured. Due to symmetry, only half of the aerator was required for the experiment. The experimental results are shown in Fig. 7, wherein, nozzle number was defined as 1 ~ 4. The bubble size was defined as horizontal width in X-direction (w_x) and vertical height in Y-direction (w_y). Measured values are tabulated in Table 1. For Configuration 2, the bubble size is always greater for nozzle 1 and 4 than it is for nozzles 2 and 3. The bubble size distribution is noticeably more uniform with Configuration 3 which in agreement with CFD results in Fig. 6. Inspection of the details in Table 1 and in particular the significant reduction in variance with Configuration 3 indicated that this is optimal in providing uniform bubbling.

3.2.2 Variation of gap distance between corrugated decks

After determining the optimal aeration pipe design, the variation of gap distance between the bottom two decks (ground decks) and the top two decks (top decks) of a CS-MBR was studied. In one of our previous studies, it is shown that slug bubble could induce effective hydrodynamics for a FS membrane height of 1500 mm [30]. Now considering that the CS membrane height is 725 mm, the ground two decks in a CS-MBR were arranged together with no gap distance (h_1), and the same was done for the upper two decks, i.e. h_1 and h_3 in Fig. S3 were set equal to zero. Thus the distance h_2 between the middle two decks (i.e., space between the second and third deck in Fig. S3) was the key variable because the processes of bubble recombination and redistribution into the upper layer of membrane modules is strongly influenced by the height of this region [30]. The distance h_2 was varied from 100 to 600 mm, with nozzle air velocity fixed at 13 m/s. Owing to the symmetric boundary, the bubble distribution and shear stress for six channels were calculated in this simulation. Channel 1 is in the center of the system positioned over the central aeration pipe, whilst channel 6 is far away from the center.

The bubble distribution and shear stress comparison are shown in Fig. 8. The results showed, as one would expect, that the gap h_2 had little influences on the hydrodynamics of the ground decks, thus a representative set of CFD results at h_2 300 mm is shown in Fig. 8 (a). In all six channels, a slug bubble with spherical cap is produced, and several small bubbles are scattered in the wake region. It shows that intense shear stress is mainly concentrated in the wake region, due to the secondary turbulence, high shear stress is also observed elsewhere. The clear finding is that for the chosen conditions and range of h_2 there would be sufficiently intense hydrodynamic effects in ground decks independent of the h_2 value.

(a)

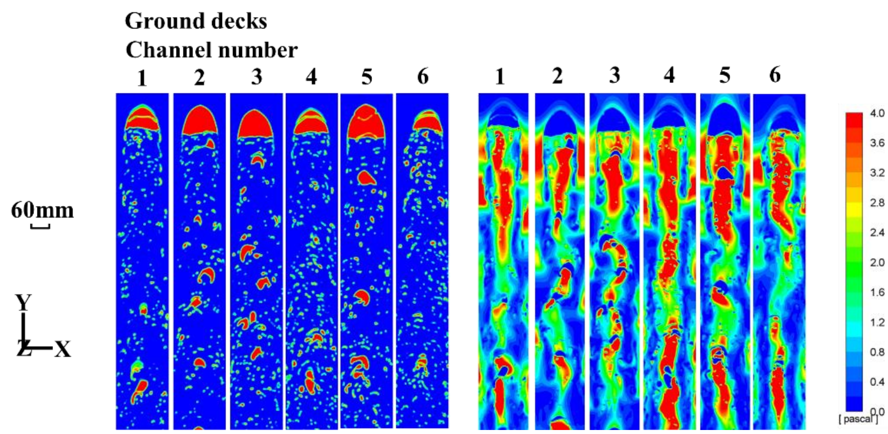

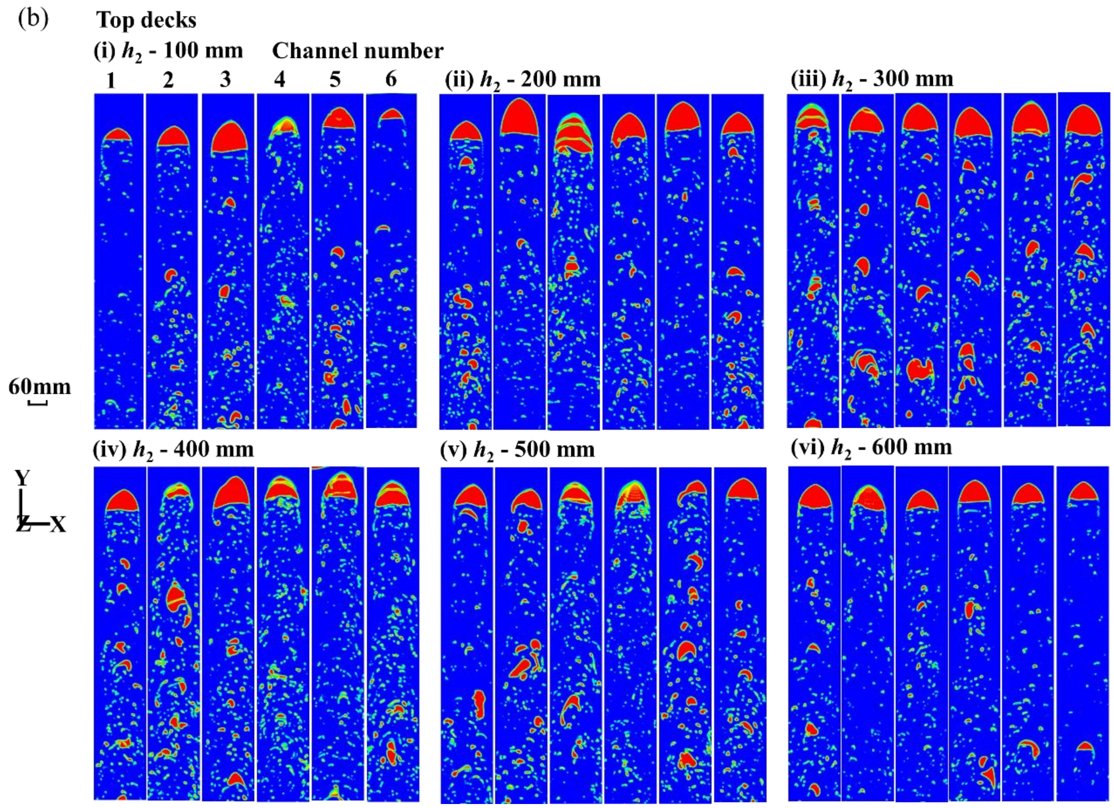
(b)
Top decks
(i) h_2 - 100 mm
Channel number
1 2 3 4 5 6
(ii) h_2 - 200 mm
(iii) h_2 - 300 mm
60mm
(iv) h_2 - 400 mm
(v) h_2 - 500 mm
(vi) h_2 - 600 mm
Y
Z
X

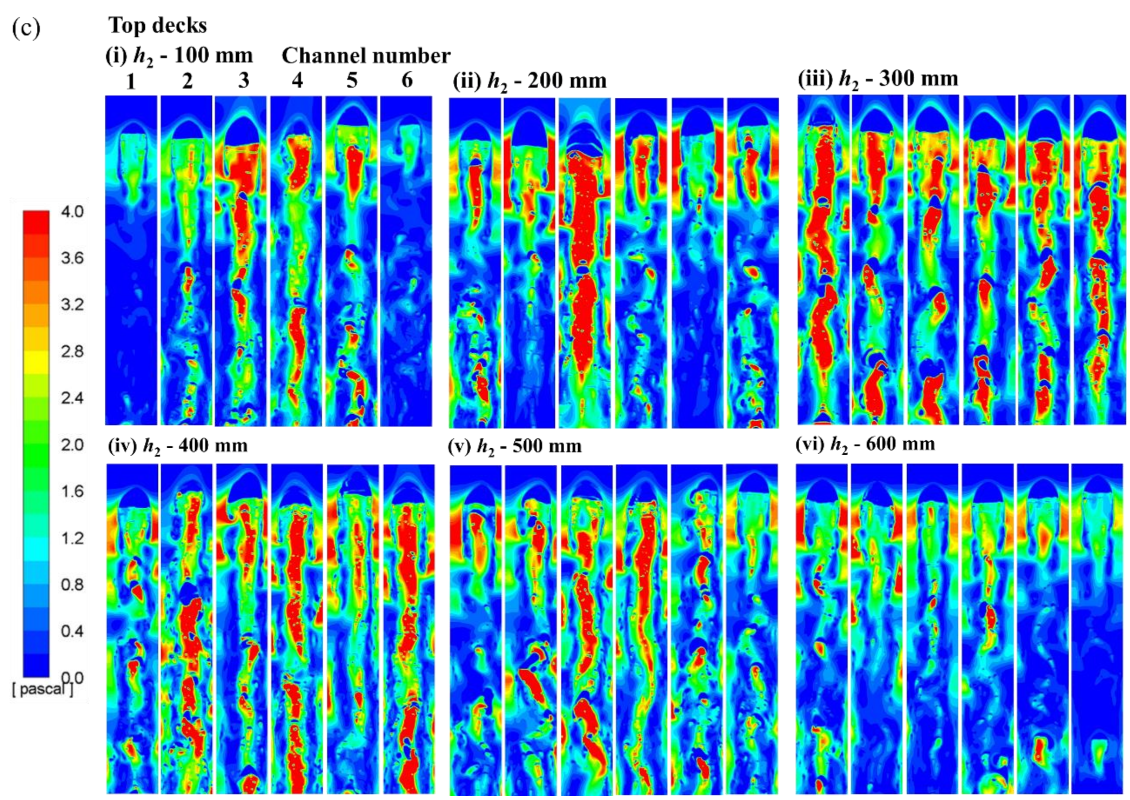
(c)
Top decks
(i) h_2 - 100 mm
Channel number
1 2 3 4 5 6
(ii) h_2 - 200 mm
(iii) h_2 - 300 mm
4.0
3.6
3.2
2.8
2.4
2.0
1.6
1.2
0.8
0.4
0.0
[pascal]
(iv) h_2 - 400 mm
(v) h_2 - 500 mm
(vi) h_2 - 600 mm

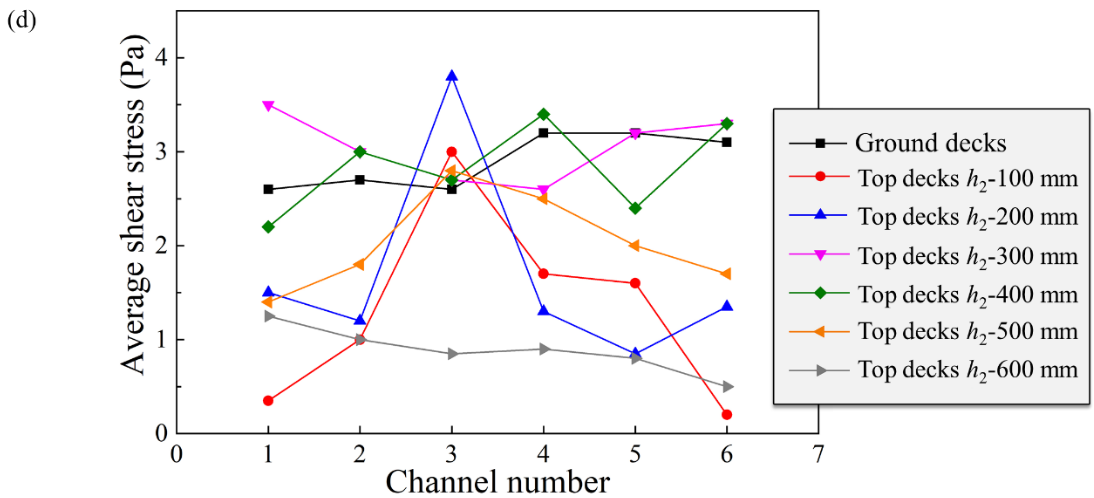

Fig. 8 Variation of gas-liquid two-phase flow and induced shear stress with channel number for various gaps of h_2: (a) distribution of slug bubbles in the lower two ground decks; (b) slug bubbles in the upper two decks; (c) shear stress on membrane walls; (d) comparison distribution of averaged shear stress in ground and top decks.

Fig. 8 (b) shows the bubble distribution in channels of the upper two decks for gap distance h_2 from 100 to 600 mm. From Case (i), h_2 = 100 mm, it illustrates that large bubbles are generated in channel 3, whilst those in other channels are small especially channels 1 and 6. Bubble size in all channels except channel 3 has increased as h_2 increased to be 200 mm in Case (ii), but it is still small for channels 1 and 6. Bubble distribution reaches an optimum in terms of uniformity as h_2 became 300 mm in Case (iii). Further the uniformity decreases as gap h_2 increases to be 400 ~ 600 mm. So overall, the bubble size and uniformity is found to vary with the gap distance h_2, and a value of 300 mm gave the greatest uniformity.

Fig. 8 (c) shows the magnitude and distribution of shear stress in different channels for each gap distance h_2. For 100 mm, Case (i), the shear stress in some regions of channel

3 reached 4 Pa, whilst there are few areas reaching 4 Pa in channels 4 and 5. However for most areas in channels 1, 2 and 6, shear stress is lower than 1 Pa. This is improved as h_2 increased to 200 mm, with the shear stress in several parts of all six membrane surfaces reaching 4 Pa, but in most regions of channel 5 it is lower than 0.5 Pa. For Cases (iii) and (iv) with h_2 300 to 400 mm, the situation is optimal in terms of shear stress distribution with most parts of all six channels having values over 1.5 Pa. At h_2 = 500 mm, the shear stress of channels 1, 2, 5 and 6 has decreased and for h_2 = 600 mm, the non-uniformity of shear stress is even more obviously.

These observations are confirmed in Fig. 8 (d) which presents the average shear stress of channels 1 to 6 in the ground and top decks under different gap distance h_2. It is presented that average shear stress of each channel in ground decks is not only greater than 2.5 Pa but there is little variation between channels. As h_2 is 300 or 400 mm, it is found that the average shear stress is over 2 Pa on membrane surfaces in top decks. For other gap distances it is lower than 1.5 Pa in some channels which would be insufficient shear stress for fouling control. Not only is the gap of 300 to 400 mm optimal to achieve uniform and an enhanced hydrodynamic effect but based upon previous work the values of shear stress will give excellent amelioration of fouling [7, 32, 39].

3.2.3 Variation of aeration rate

For industry, air velocity is an important variable as it is directly related to the aeration cost and system operation [26, 40, 41]. In this section, hydrodynamic effect was studied at five nozzle flow velocities, which were shown in Figs. 9 and 10 for ground and top decks respectively.

In Fig. 9 (a), clearly at a nozzle velocity 10 m/s in Case (i), the bubbles generated in the ground decks are not uniform, and are especially small in Channel 6. As the nozzle velocity increases from 11.5 to 16 m/s, the bubble size increases and the uniformity becomes better amongst different channels. The magnitude of shear stresses on membrane walls are shown in Fig.9 (b). Clearly, at velocities of 13 to 14.5 m/s the shear stresses generated in most regions of all channels are uniform and could reach up to 4 Pa. At lower velocities, the shear stresses in most regions of channels 1 and 6 are less than 1 Pa. Also at higher velocities of 16 m/s, the uniformity of distribution becomes worse compared with the mid-range velocities. This is confirmed by Fig. 9 (c). Clearly for the ground decks, the optimal nozzle velocity is in the range 13 to 14.5 m/s; the results for these two velocities are shown with thicker lines in Fig. 9 (c).

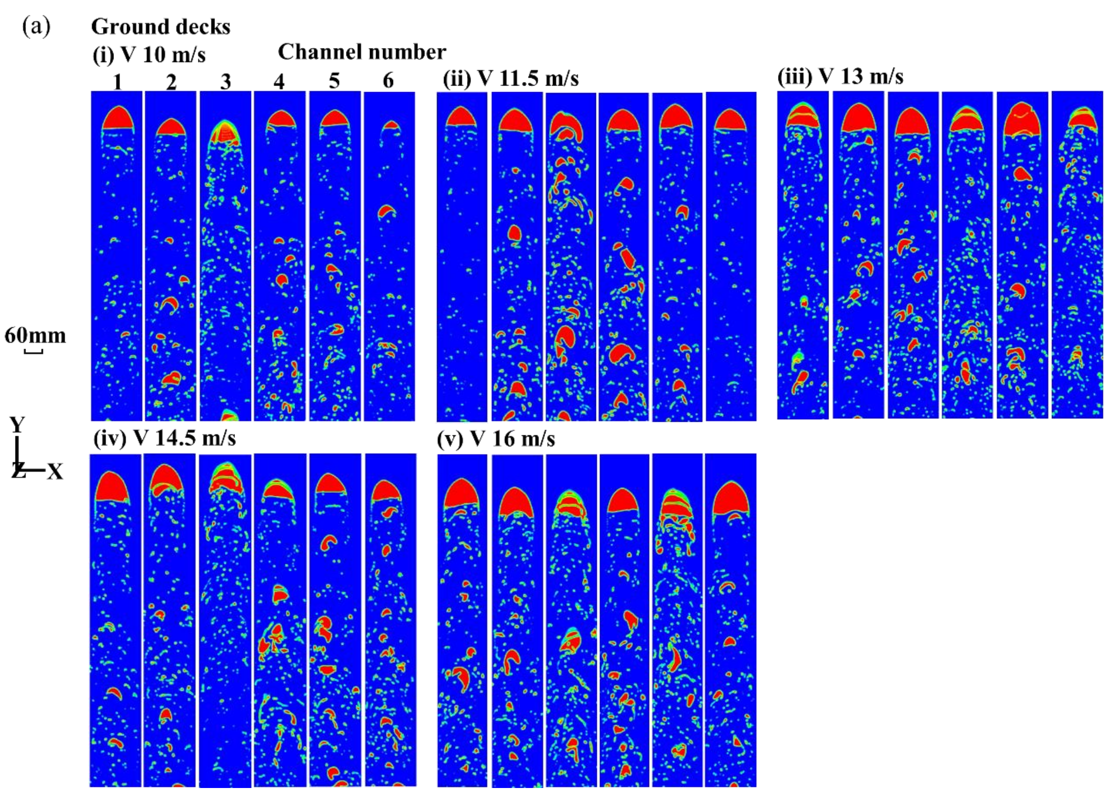

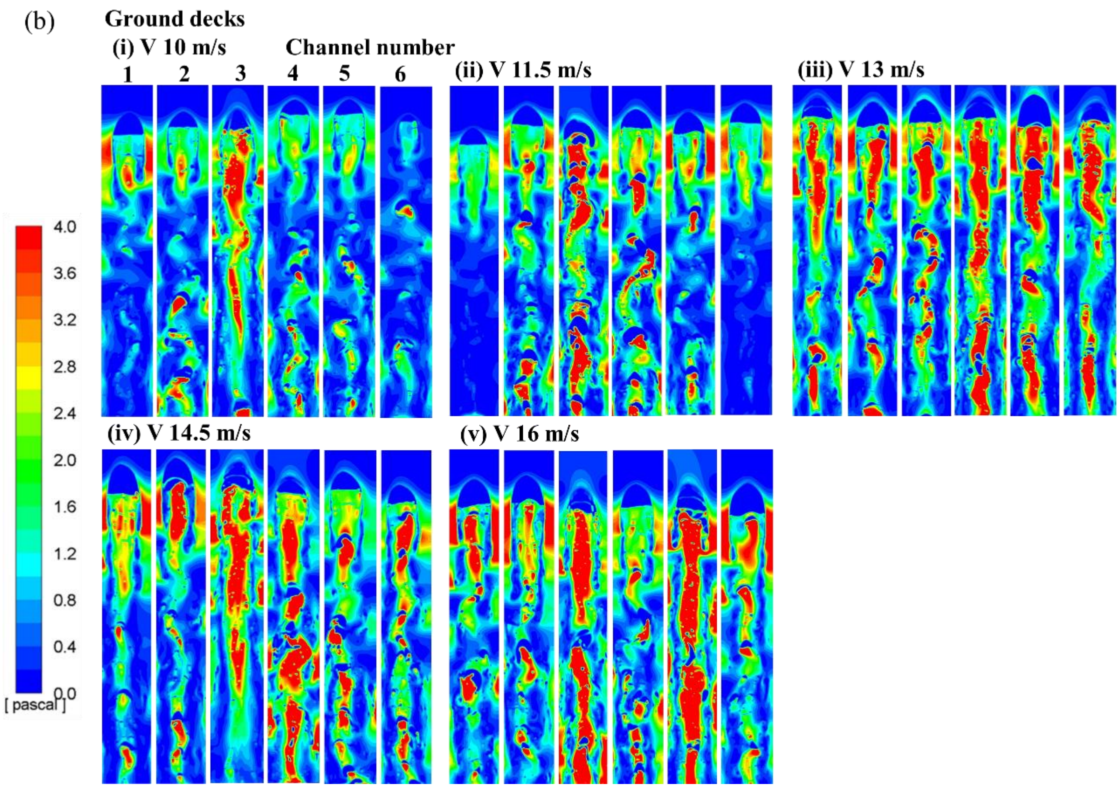

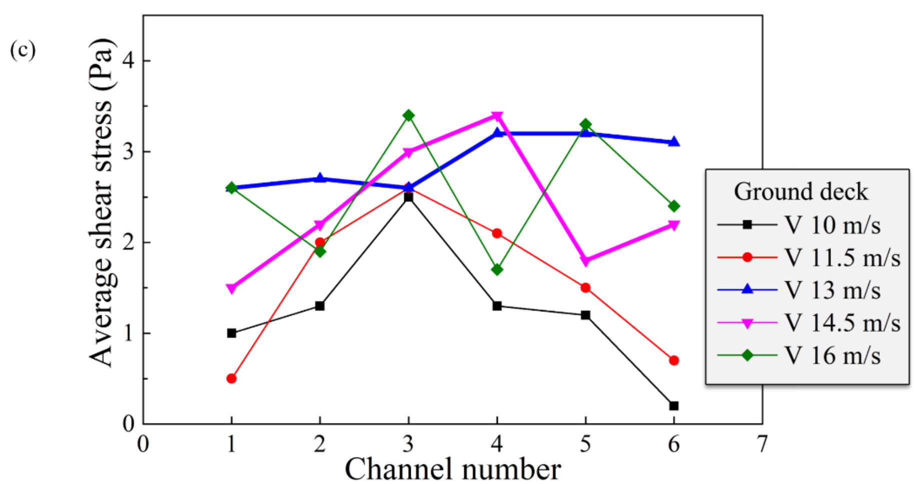

Fig. 9 Variation of gas-liquid two-phase flow and induced shear stress with channel number for ground decks at various air nozzle velocities: (a) distribution of slug bubbles in the lower two ground decks; (b) shear stress distribution; (c) averaged shear stress.

For top decks, variation of bubble distribution and shear stress are shown in Fig. 10. As with the lower two decks, a velocity of less than 13 m/s has regions where shear stress < 0.4 Pa e.g. in channels 1, 2 and 6. Furthermore the average value of shear stress varies with channel number and is less than 1.5 Pa in more than 4 channels, as shown in Fig. 10 (c). It is more uniform at 13 ~ 16 m/s nozzle velocity and the average values of shear stress are over 2.5 Pa for six channels.

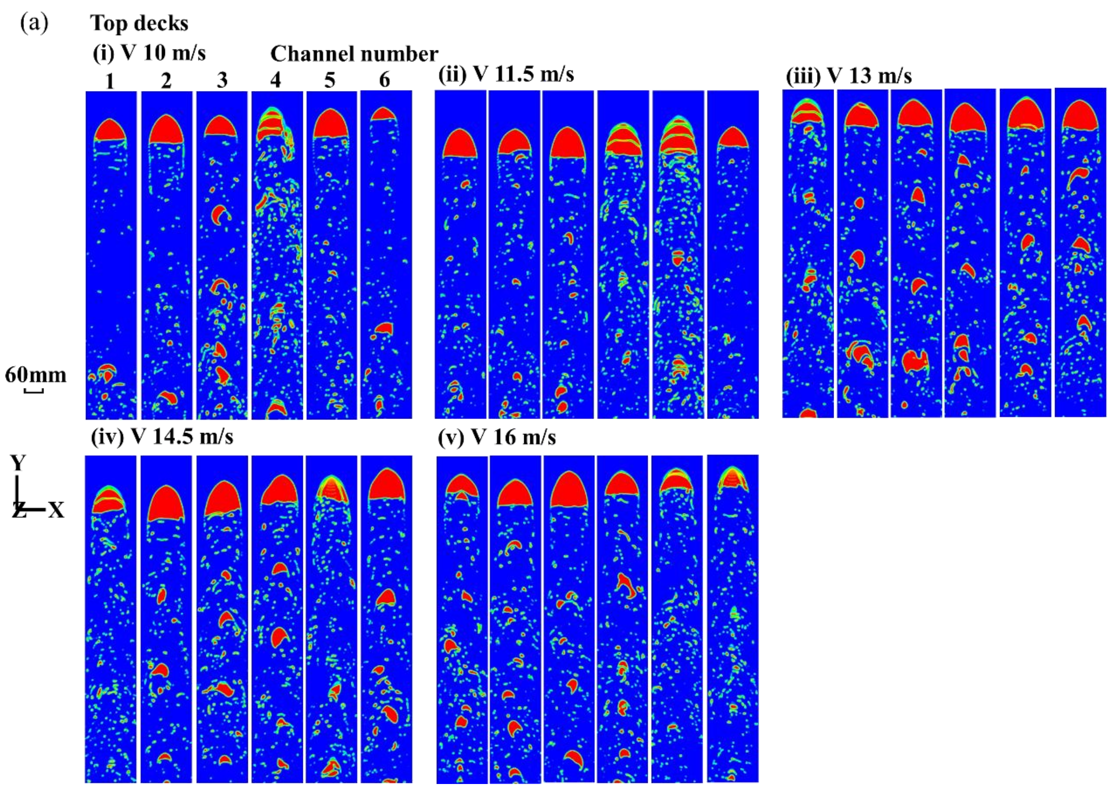

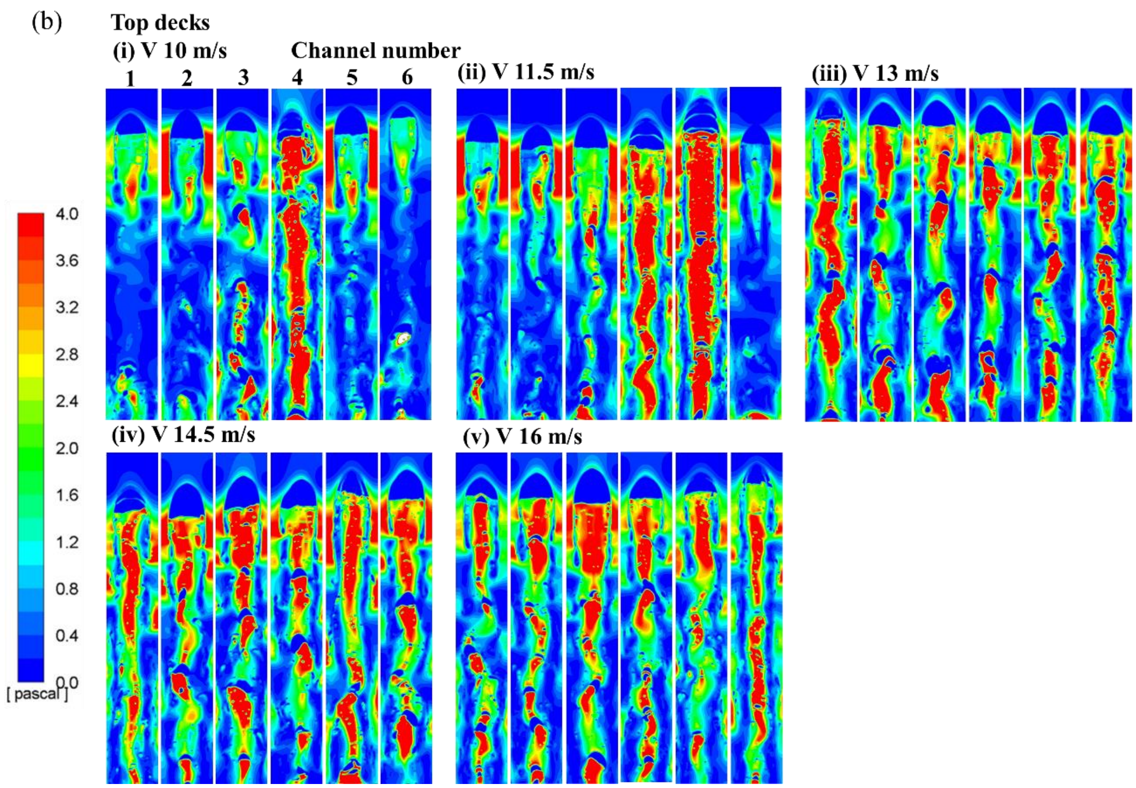

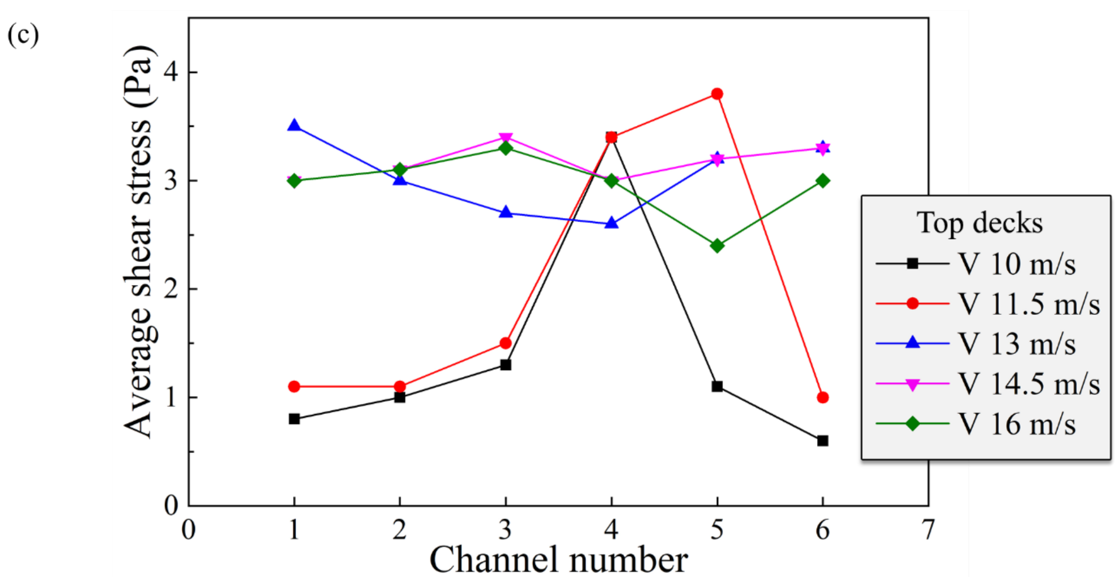

Fig. 10 Bubble distribution and induced shear stress in top decks for various air nozzle velocities: (a) distribution of slug bubbles; (b) shear stress on membrane walls; (c) averaged shear stress.

Overall, by reviewing distribution of bubbles and shear stress through both ground and top decks, the most uniform and intense hydrodynamic effect is produced at nozzle velocities between 13 and 14.5 m/s. Hence, this is the optimal range beneficial for fouling control performance.

3.3 Air consumption

Based on those optimal design of MBR variables, we can estimate aeration cost of a CS-MBR operated so as to have an average shear stress greater than 1.5 Pa in all channels. At the optimal operating conditions of h_2 300 mm and nozzle velocity 13 m/s, the membranes in 12 channels would have surface shear stress over 1.5 Pa, which indicates they could be all effectively covered by one aeration pipe. Based on these optimal design conditions, air consumption for four- and six-deck CS-MBRs were calculated.

Table 2 Comparison of air consumption in slug bubbling Corrugated Sheet MBRs.

Number of Decks	Number of channels covered by one aeration pipe	SAD_m ($Nm^3m^{-2}h^{-1}$)	Air flow rate per m^2 (L/min·m^2)	Air flow rate per deck (L/min·deck)	Saving in air consumption (%)*
Multi-deck CS-MBR includes corrugated sheet membranes sized 725 × 1320 × 1.6 mm (L×W×T), with channel gap 5 mm. Each deck includes 100 sheets.					
4	12	0.074	1.37	286	86
6	12	0.049	0.91	190	91
FSMBR includes 100 flat sheets of membranes sized 1200 × 510 × 5 mm (L×W×T), with channel gap 5 mm [41].					
1	12	0.29	5.02	590	50

* These are estimates based upon industrial air usage of 10 L/min·m^2.

As shown in Table 2, the specific aeration demand per membrane area, SAD_m for four-deck CS-MBR is 0.074 $Nm^3m^{-2}h^{-1}$, whilst the estimate for a six-deck CS-MBR is 0.049 $Nm^3m^{-2}h^{-1}$. The air flow rate per square meter is 0.91 ~ 1.37 L/min·m^2, which is much lower than 10 L/min·m^2 for FSMBR in industry and lower than the figure given for a HFMBR by Verrecht et al. [20]. According to our previous research, the optimized FSMBR could save 50% of air consumption compared to the traditional industrial air consumption, whilst the four-deck and six-deck CS-MBR could save 86% and 91% of the air consumption, respectively. This indicates that the CS-MBR reduces around 70% air consumption than the FSMBR to achieve effective hydrodynamics for fouling control.

3.4 Discussion

Patterning or other modification of the shape of a membrane surface has been explored for more than 20 years. The approach of most research is to make ripples on the flat membrane through different methods to induce intense turbulence and increase the membrane area [42]. In most studies, the ripples structure on membrane surface has been found to be beneficial for fouling control bringing benefits such as enhanced shear stress, less filter cake, larger filtration flux, etc. [37]. The hydrodynamics induced by corrugations have also been found to be beneficial in limiting salt deposition in membrane distillation [42, 43]. Our findings on fouling are consistent with these previous findings.

In the current work not only is the membrane surface improved but the membrane supporting pattern, thickness and water conveyance has also been modified. The new CS membrane has unique features combining some characteristics from both HF and FS membranes characteristics. The unique features of CS membrane studied in this work are summarized and compared in Table 3. For non-flat membrane, the surface area distinction was reported by Barambu et al. [44]. In this work, the area for corrugated sheet is taken as the actual area by considering the corrugated shape, which is 1.1 times that of a flat sheet with the same projected area. The greater area will give a lower local flux which according to critical flux theory [45] (and threshold flux theory [46]) will give less fouling. Decoupling this contribution from the hydrodynamics is difficult. However from an engineering perspective, the important parameters are: (a) SAD_m and (b) productivity per unit volume (I.e. amount of permeate per unit volume of the MBR). Hence, the advantage of corrugated membrane is due to both points of larger area and stronger hydrodynamics. The SAD_m value is based upon 4 decks and it will be recalled that in section 3.2.2 the height of 4 CS decks is equivalent to the height of two FS decks. Thus the comparison between flat and corrugated in Table 3 is a fair one.

Table 3 Feature summary and comparison of CS membrane system with others

Surface configuration	Flat	Corrugated in this study	Corrugated by Kharraz et al. [42]
Corrugation fabricate mothed	N/A	Hemispherical hollow units fixed on plate	Physically press
Membrane surface area (m^2)	1	1.1	0.012
Membrane support method	Frame	PET plate	Frame
Membrane thickness (mm)	7	1.6	6
Water conveyance	Traditionally upright	Horizontally along corrugated channels	upright
MBR	1 ~ 2 decks	generally 4 decks	one sheet (lab-scale exp.)

Aeration consumption (L/min·m^2)	5.02 [39] 10 (traditional usage)	1.37	166 (lab-scale exp.)

The features of the CS membrane assembly mentioned above are particularly beneficial for large-scale application. For example, the small thickness of CS membrane could increase the loading capacity and solving the low-capacity issue faced in FSMBR application. Moreover, the general plane sheet configuration of the CS membrane provides a format that avoids any clogging such as that found when fibers bind ("hair twinning") in HFMBRs. Furthermore the aspect ratio of the CS-MBR creates the possibility of having multiple decks which significantly reduce the air consumption, that are at a world-leadingly low level. For these multiple reasons the CS-MBR format is an exciting new prospect in the industrial application of MBRs.

4. Conclusions

A novel corrugated membrane format with a surface area per unit volume value equivalent to that of hollow fiber MBR systems has been evaluated, and a design of a multi-deck CS-MBR elaborated. Specific conclusions arising from the experimental and simulation investigations are:

1) From a comparison of the hydrodynamics and related fouling performance of the new CS membrane system with the FS membrane system, it is established that the surface shear stress induced on the CS membrane could be 1.25 times larger than that of FS. Under the same experimental conditions, the required TMP in a CS-MBR is two-thirds of that required in a FS-MBR under comparable conditions. The enhanced

hydrodynamic effect of intense turbulence and shear stress is beneficial for membrane fouling control.

2) For optimal performance a large-scale CS-MBR should have the following features: (a) be designed with a "fully partitioned" aeration pipe so as to have as uniform an air velocity distribution as possible; (b) be designed with at least four decks; (c) for a four-deck system have essential zero gap between the lower two and upper two decks and a gap of 300 mm in the middle of the system, i.e. values of h_1, h_2, h_3 are 0, 300, 0 mm respectively; and (d) have a design nozzle velocity of 13 m/s which together with an "fully partitioned" aeration pipe will ensure a small variance of 1.4 m/s. Overall an essentially uniform distributions of slug bubbles will generate sufficiently intense shear stress on membrane surfaces.
3) The standardized aeration rate, SAD_m, for the large-scale CS-MBR system can be 0.074 $Nm^3m^{-2}h^{-1}$, which corresponds to a 70% reduction with respect to an optimized FSMBR operated with slug bubbling. The value of 0.074 $Nm^3m^{-2}h^{-1}$ represents a massive reduction with respect to the traditional industrial usage of 0.58 $Nm^3m^{-2}h^{-1}$.

Given these specific findings, this new type of corrugated membrane has great potential to widen the application of flat-sheet MBR systems. Achieving a good balance between (i) having a drastically reduced air consumption and (ii) excellent fouling control should be readily achievable because it has been found in our evaluation that the new corrugated membrane benefits both areas. With more difficult-to-treat streams it may be necessary to take a smaller benefit with regard to air consumption in order to achieve good fouling control.

Acknowledgements

This work was supported by grants from National Natural Science Foundation of China (No. 52100047); National Natural Science Foundation of China (No. 21706221). RWF acknowledges the support provided by an APEX project on water reuse that has been supported by the Royal Society in partnership with the British Academy and the Royal Academy of Engineering together with generous support from the Leverhulme Trust. We would like to thank Dr. Shuren Chou and Dr. Pan Dai from Beijing Origin Water Membrane Technology Co. Ltd for their comments, help, and assistance.

References

[1] C. Wang, T.C.A. Ng, H.Y. Ng, Comparison between novel vibrating ceramic MBR and conventional air-sparging MBR for domestic wastewater treatment: Performance, fouling control and energy consumption, Water Research, 203 (2021) 117521.

[2] P. Le-Clech, V. Chen, T.A.G. Fane, Fouling in membrane bioreactors used in wastewater treatment %J Journal of Membrane Science, 284 (2006).

[3] H. He, X. Xin, W. Qiu, D. Li, Z. Liu, J. Ma, Role of nano-Fe3O4 particle on improving membrane bioreactor (MBR) performance: Alleviating membrane fouling and microbial mechanism, Water Research, 209 (2022) 117897.

[4] H. Sun, H. Liu, S. Wang, F. Cheng, Y. Liu, Ceramic membrane fouling by dissolved organic matter generated during on-line chemical cleaning with ozone in MBR, Water Research, 146 (2018) 328-336.

[5] Z.F. Cui, Experimental investigation on enhancement of crossflow ultrafiltration with air sparging, Effective Membrane Processes—New Perspectives., Mechanical Engineering Publications Ltd, London, (1993) 237–245.

[6] Z.F. Cui, S. Chang, A.G. Fane, The use of gas bubbling to enhance membrane processes, Journal of Membrane Science, 221 (2003) 1-35.

[7] K. Zhang, Z. Cui, R. Field, Effect of bubble size and frequency on mass transfer in flat sheet MBR, Journal of Membrane Science, 332 (2009) 30-37.

[8] J.A. Gil, L. Túa, A. Rueda, B. Montaño, M. Rodríguez, D. Prats, Monitoring and analysis of the energy cost of an MBR, Desalination, 250 (2010) 997-1001.

[9] K. Xiao, S. Liang, X. Wang, C. Chen, X. Huang, Current state and challenges of full-scale membrane bioreactor applications: A critical review, Bioresource Technology, 271 (2019) 473-481.

[10] K. Nam, S. Heo, G. Rhee, M. Kim, C. Yoo, Dual-objective optimization for energy-saving and fouling mitigation in MBR plants using AI-based influent prediction and an integrated biological-physical model, Journal of Membrane Science, 626 (2021) 119208.

[11] F. Meng, S. Zhang, Y. Oh, Z. Zhou, H.-S. Shin, S.-R. Chae, Fouling in membrane bioreactors: An updated review, Water Research, 114 (2017) 151-180.

[12] T. Gao, K. Xiao, J. Zhang, X. Zhang, X. Wang, S. Liang, J. Sun, F. Meng, X. Huang, Cost-benefit analysis and technical efficiency evaluation of full-scale membrane bioreactors for wastewater treatment using economic approaches, Journal of Cleaner Production, 301 (2021) 126984.

[13] M. Brannock, G. Leslie, Y. Wang, S. Buetehorn, Optimising mixing and nutrient removal in membrane bioreactors: CFD modelling and experimental validation, Desalination, 250 (2010) 815-818.

[14] J. Hashisho, M. El-Fadel, M. Al-Hindi, D. Salam, I. Alameddine, Hollow fiber vs. flat sheet MBR for the treatment of high strength stabilized landfill leachate, Waste Management, 55 (2016) 249-256.

[15] T.-T. Nguyen, X.-T. Bui, V.-P. Luu, P.-D. Nguyen, W. Guo, H.-H. Ngo, Removal of antibiotics in sponge membrane bioreactors treating hospital wastewater: Comparison between hollow fiber and flat sheet membrane systems, Bioresource Technology, 240 (2017) 42-49.

[16] T. Sano, Y. Koga, H. Ito, L.V. Duc, T. Hama, Y. Kawagoshi, Effects of structural vulnerability of flat-sheet membranes on fouling development in continuous submerged membrane bioreactors, Bioresource Technology, 304 (2020) 123015.

[17] E. Radaei, X. Liu, K.H. Tng, G. Merendino, F.J. Trujillo, P.R. Bérubé, G. Leslie, Numerical and experimental investigation of pulse bubble aeration with high packing density hollow-fibre MBRs, Water Research, 160 (2019) 60-69.

[18] J.A. Kharraz, M.R. Bilad, H.A. Arafat, Flux stabilization in membrane distillation desalination of seawater and brine using corrugated PVDF membranes, Journal of Membrane Science, 495 (2015) 404-414.

[19] X. Liu, Y. Wang, Y. Shi, Q. Li, P. Dai, J. Guan, T.D. Waite, G. Leslie, CFD modelling of uneven flows behaviour in flat-sheet membrane bioreactors: From bubble generation to shear stress distribution, Journal of Membrane Science, 570-571 (2019) 146-155.

[20] B. Verrecht, T. Maere, I. Nopens, C. Brepols, S. Judd, The cost of a large-scale hollow fibre MBR, Water research, 44 (2010) 5274-5283.

[21] R. Field, K. Zhang, Z. Cui, B.-K. Hwang, Flat sheet MBRs: Analysis of TMP rise and surface mass transfer coefficient, Desalination and Water Treatment, 35 (2011) 82-91.

[22] Y. Wang, J. Howell, R. Field, D. Wu, Simulation of Cross-Flow Filtration for baffled tubular channels and pulsatile flow, Journal of Membrane Science, 95 (1994) 243-258.

[23] A. M. Gronda , S. Buechel, E. L. Cussler, Mass Transfer in Corrugated Membranes, Journal of Membrane Science, 165(2) (2000) 177-187.

[24] A. Fenu, J. Roels, T. Wambecq, K. De Gussem, C. Thoeye, G. De Gueldre, B. Van De Steene, Energy audit of a full scale MBR system, Desalination, 262 (2010) 121-128.

[25] M.W.D. Brannock, H. De Wever, Y. Wang, G. Leslie, Computational fluid dynamics simulations of MBRs: Inside submerged versus outside submerged membranes, Desalination, 236 (2009) 244-251.

[26] K. Zhang, P. Wei, M. Yao, R.W. Field, Z. Cui, Effect of the bubbling regimes on the performance and energy cost of flat sheet MBRs, Desalination, 283 (2011) 221-226.

[27] B. Wang, Y. Zhang, G. Zhang, K. Zhang, R. Field, Innovation and optimization of aeration in free bubbling flat sheet MBRs, Journal of Membrane Science, 635 (2021) 119522.

[28] B. Wang, Y. Zhang, Y. Fang, K. Zhang, R.W. Field, Aeration pipe design for free bubbling hydrodynamic optimization of flat sheet MBRs, Journal of Membrane Science, 646 (2022) 120222.

[29] M. Yang, D. Yu, M. Liu, L. Zheng, X. Zheng, Y. Wei, F. Wang, Y. Fan, Optimization of MBR hydrodynamics for cake layer fouling control through CFD simulation and RSM design, Bioresource Technology, 227 (2017) 102-111.

[30] B. Wang, K. Zhang, R.W. Field, Novel economical three-stage slug bubbling process in a large-scale flat-sheet membrane bioreactor of double deck configuration, AIChE Journal, 66 (2020).

[31] G. Ducom, F.P. Puech, C. Cabassud, Air sparging with flat sheet nanofiltration: a link between wall shear stresses and flux enhancement, Desalination, 145 (2002) 97-102.

[32] P. Wei, K. Zhang, W. Gao, L. Kong, R. Field, CFD modeling of hydrodynamic characteristics of slug bubble flow in a flat sheet membrane bioreactor, Journal of Membrane Science, 445 (2013) 15-24.

[33] M. Dalmau, H. Monclús, S. Gabarrón, I. Rodriguez-Roda, J. Comas, Towards integrated operation of membrane bioreactors: Effects of aeration on biological and filtration performance, Bioresource Technology, 171 (2014) 103-112.

[34] X. Du, X. Liu, Y. Wang, E. Radaei, B. Lian, G. Leslie, G. Li, H. Liang, Particle deposition on flat sheet membranes under bubbly and slug flow aeration in coagulation-microfiltration process: Effects of particle characteristic and shear stress, Journal of Membrane Science, 541 (2017) 668-676.

[35] C. Gaucher, P. Legentilhomme, P. Jaouen, J. Comiti, J. Pruvost, Hydrodynamics study in a plane ultrafiltration module using an electrochemical method and particle image velocimetry visualization, Experiments in Fluids, 32 (2002) 283-293.

[36] P.R. Bérubé, G. Afonso, F. Taghipour, C.C.V. Chan, Quantifying the shear at the surface of submerged hollow fiber membranes, Journal of Membrane Science, 279 (2006) 495-505.
[37] K. Scott, A.J. Mahmood, R.J. Jachuck, B. Hu, Intensified membrane filtration with corrugated membranes, Journal of Membrane Science, 173 (2000) 1-16.
[38] R. Field, J. Wu, Modelling of permeability loss in membrane filtration: Re-examination of fundamental fouling equations and their link to critical flux, Desalination, 283 (2011).
[39] B. Wang, K. Zhang, R. Field, Novel Aeration of a large-scale flat sheet MBR: a CFD and experimental investigation, AIChE Journal, 64 (2018).
[40] B. Wang, K. Zhang, R.W. Field, Optimization of aeration variables in a commercial large-scale flat-sheet MBR operated with slug bubbling, Journal of Membrane Science, 567 (2018) 181-190.
[41] B. Wang, K. Zhang, R.W. Field, Slug bubbling in flat sheet MBRs: Hydrodynamic optimization of membrane design variables through computational and experimental studies, Journal of Membrane Science, 548 (2018) 165-175.
[42] J.A. Kharraz, M.R. Bilad, H.A. Arafat, Simple and effective corrugation of PVDF membranes for enhanced MBR performance, Journal of Membrane Science, 475 (2015) 91-100.
[43] Y. Elhenawy, N. Elminshawy, M. Bassyouni, et al., Experimental and theoretical investigation of a new air gap membrane distillation module with a corrugated feed channel, Journal of Membrane Science, 594 (2019) 117461.

[44] N. Barambu, M. Bilad, A. Laziz, et al., A wavy flow channel system for membrane fouling control in oil/water emulsion filtration, Journal of Water Process Engineering, 44 (2021) 102340.

[45] R.W. Field, D. Wu, J.A. Howell, B.B. Gupta, Critical flux concept for microfiltration fouling, Journal of Membrane Science, 100, 259-272, 1995

[46] R.W. Field, G.K. Pearce Critical, sustainable and threshold fluxes for membrane filtration with water industry applications, Advances in Colloid and Interface Science, 164, 38-44, 2011